Published in final edited form as:
J Microsc. 2009 January ; 233(1): 114–131. doi:10.1111/j.1365-2818.2008.03102.x.

Automated identification of neurons in 3D confocal datasets from zebrafish brainstem

M. KAMALI[*], **L. J. DAY**[†], **D. H. BROOKS**[*], **X. ZHOU**[‡], and **D. M. O'MALLEY**[†]

[*] Department of Electrical and Computer Engineering, Boston, Massachusetts, U.S.A.

[†] Department of Biology, Northeastern University, Boston, Massachusetts, U.S.A.

[‡] Department of Radiology & Bioinformatics Core, Methodist Hospital Research Institute, Houston, Texas, U.S.A.

Summary

Many kinds of neuroscience data are being acquired regarding the dynamic behaviour and phenotypic diversity of nerve cells. But as the size, complexity and numbers of 3D neuroanatomical datasets grow ever larger, the need for automated detection and analysis of individual neurons takes on greater importance. We describe here a method that detects and identifies neurons within confocal image stacks acquired from the zebrafish brainstem. The first step is to create a template that incorporates the location of all known neurons within a population – in this case the population of reticulospinal cells. Once created, the template is used in conjunction with a sequence of algorithms to determine the 3D location and identity of all fluorescent neurons in each confocal dataset. After an image registration step, neurons are segmented within the confocal image stack and subsequently localized to specific locations within the brainstem template – in many instances identifying neurons as specific, individual reticulospinal cells. This image-processing sequence is fully automated except for the initial selection of three registration points on a maximum projection image. In analysing confocal image stacks that ranged considerably in image quality, we found that this method correctly identified on average ~80% of the neurons (if we assume that manual detection by experts constitutes 'ground truth'). Because this identification can be generated approximately 100 times faster than manual identification, it offers a considerable time savings for the investigation of zebrafish reticulospinal neurons. In addition to its cell identification function, this protocol might also be integrated with stereological techniques to enhance quantification of neurons in larger databases. Our focus has been on zebrafish brainstem systems, but the methods described should be applicable to diverse neural architectures including retina, hippocampus and cerebral cortex.

Keywords

Database; fluorescence; Hough; lesion; phenotype; reticulospinal; segmentation; spinal; stereology; tracing; vertebrate

Introduction

Vertebrate central nervous systems contain hundreds or thousands of distinct nerve cell types with specialized morphologies and functions. Because neural systems are disrupted in diverse situations including neurodegenerative diseases, stroke and spinal cord injury, it is important to understand the organization of these systems. But neuroscience researchers face major

Correspondence to: Donald M. O'Malley. Tel: 617-373-2284; fax: 617-373-3724; d.omalley@neu.edu.

technical obstacles in terms of identifying individual nerve cells. For example, one cannot yet say with certainty how many types of nerve cells there are in the central nervous system (CNS) of different mammals (MacNeil & Masland, 1998; Stevens, 1998; Masland, 2001; Maccaferri & Lacaille, 2003; Nelson *et al.*, 2006a,b) or even in lower vertebrate nervous systems (Davis & McClellan, 1994; Buchanan *et al.*, 2001; Deliagina *et al.*, 2002; Baez *et al.*, 2003; Benito-Gutierrez, 2006). This situation hinders our understanding of how neuronal populations process sensory information, make decisions and execute motor programs. More robust and efficient identification schemes would enhance our knowledge base and would facilitate efforts to repair and reconstruct damaged neural systems.

Diverse kinds of neuron-specific information are used and needed by researchers. For example, morphological information and synaptic connectivity provide clues concerning the integrative capacity of nerve cells and their specific role within a given neural network. The activity patterns of neurons, including electrical and chemical activities, as well as slower changing patterns of gene expression, provide further information about neural operations. There are voluminous data of these sorts (see, e.g. Herdegen & Leah, 1998; Li, 2001; Gong *et al.*, 2003; Hochheiser & Yanowitz, 2007), but it is often difficult to relate data obtained in one experiment (e.g. in an electrophysiology experiment) to data obtained in other experiments (e.g. morphological or gene expression experiments) (Yen & Jones, 1983; Okazaki *et al.*, 2001; De Filipe, 2004; Gal *et al.*, 2006; Jinno *et al.*, 2007; Marmigere & Ernfors, 2007; Schulz *et al.*, 2007). This is because of the vast numbers of neurons in the CNS (numbering in the billions in some mammals) and the great complexity of the neural architectures containing these cells. It becomes an overwhelming problem to manually examine large neural datasets, extract relevant information and relate data obtained in different kinds of experiments – or even in replicates of the same experiment.

One step towards solving this problem has been the creation of neuronal databases. A cell-centred database has been created that organizes electron- and light-microscopic information and encourages annotation of both subcellular and multicellular structures, including, e.g. dendritic-branching patterns and the organization of the node of Ranvier (Martone *et al.*, 2003, 2008). Another database called the brain architecture knowledge management system provides an easy means of making neuroanatomical queries within a framework that includes both physical descriptions and computational models (Bota *et al.*, 2005; Bota & Swanson, 2007). The CoCoDat database (collation of cortical data) focuses on morphological data, connectivity and physiological data pertaining to mammalian neocortical neurons (Dyhrfjeld-Johnsen *et al.*, 2005). The impact of neuronal heterogeneity on the information carrying capacity of such systems has recently been investigated (Shamir & Sompolinsky, 2006). With regard to unique, individually identifiable neurons, Calin-Jageman *et al.* (2007) have attempted to codify diverse experimental data from invertebrate animals. Studies of individually identified neurons have led to major insights into the operations of neural circuits in marine snails, crustaceans, leeches and insects (see, e.g. Kupfermann & Kandel, 1969; Friesen *et al.*, 1978; Cazalets *et al.*, 1990; Katz & Harris-Warrick, 1990; Boyan *et al.*, 1995; Urban & Technau, 1997; Schulz *et al.*, 2007). Systematic analysis becomes more essential in the case of vertebrate animals, whose neurons can number in the billions, but current techniques do not allow for the automated identification of vertebrate neurons.

Individually identified vertebrate neurons have traditionally been recognized by manually identifying them in light micrographs or inside living animals. This has been done most extensively in the brainstem and spinal cord of lamprey (Rovainen, 1967; Mackler & Selzer, 1987; Swain *et al.*, 1995; Buchanan, 2001) and zebrafish (Kimmel *et al.*, 1982; Bernhardt *et al.*, 1990; Fetcho & O'Malley, 1995; Fetcho *et al.*, 1998; Gahtan *et al.*, 2002; Lewis & Eisen, 2003). Most prominent among the vertebrate identified neurons are the Mauthner cells, of which there are just two in the entire brain (Furukawa & Furshpan, 1963; Eaton & Farley,

1975; Korn & Faber, 1975). The Mauthner cell and its segmental homologues have been examined by a wide variety of methods (Zottoli, 1977; Metcalfe *et al.*, 1986; O'Malley *et al.*, 1996; Liu & Fetcho, 1999; Eaton *et al.*, 2001; Gahtan & O'Malley, 2003; Nakayama & Oda, 2004). The foregoing examples are part of a larger body of work on identified vertebrate neurons (see, e.g. Bernhardt *et al.*, 1990; Friedrich & Korsching, 1997; Drapeau *et al.*, 1999; Hale *et al.*, 2001; Gahtan & O'Malley, 2001; Deliagina *et al.*, 2002; Gahtan *et al.*, 2005; Niell & Smith, 2005; Severi *et al.*, 2007; Orger *et al.*, 2008).

We focus here on an array of descending neurons in the 7-day-old larval zebrafish. The spinal-projecting neurons of these larvae number approximately 300 in total – 150 on each side of the brainstem. Large-scale analysis of this neuronal population (referred to as the descending motor control system) is hindered by the difficulty of recognizing specific individual neurons across datasets. We address this issue in the context of labelled-lesion experiments (Gahtan & O'Malley, 2001) where large numbers of descending neurons are axotomized and fluorescently labelled. The sets of neurons labelled, however, are highly variable and their identities are unknown in the absence of expert identification. Because maximum intensity projections (MIPs) do not provide sufficient information for cell identification, one must, in most cases, manually and repeatedly navigate through a number of confocal image stacks (or 'z-stacks') to identify the neurons present in each fish. Performing this same procedure for many confocal datasets is time consuming and mentally fatiguing, given the many dozens or even hundreds of neurons that must be identified. Having a computer algorithm that could systematically carry out such tasks by mimicking the manual identification procedure should increase both experimental throughput and accuracy. Although we are focusing on the zebrafish brainstem as a test-bed for this cell identification protocol, this approach is potentially adaptable to nerve cell identification in a variety of neural systems.

Materials and methods

There are many approaches to segmentation and transformation of neural structures, especially in the area of human brain mapping (Brown, 1992; van den Elsen *et al.*, 1993; Davatzikos *et al.*, 1996; Joshi & Miller, 2000). Such approaches as elastic warping (Gee & Bajcsy, 1998; Machado & Gee, 2003) and the use of linear elastic and viscous models (Christensen *et al.*, 1994) play an important role in the analysis of macroscopic neuroanatomical datasets. In some cases, the segmentation and registration functions may be combined using a Bayesian approach (Fischl *et al.*, 2002), whereas artificial networks have been used to segment cell layers (Ruggeri & Pajaro, 2002). A distinct family of 'stereological' techniques aims to quantify neuronal densities via specialized sampling methods (Popken & Farel, 1997; Howard & Reed, 1998; Geuna, 2000, 2005; Ma *et al.*, 2003), but generally these techniques are not automated. For our purposes, automation at the level of neural circuits and individual nerve cells is essential. The dynamic behaviours of neurons can be quantified by selecting appropriate Bayesian models (Al-Kofahi *et al.*, 2006). It is also possible to trace neuronal processes in noisy confocal datasets (Al-Kofahi *et al.*, 2003a,b). Other automated approaches to analysing 3D structures included the tracking of vasculature using a Hough transform (Barber *et al.*, 2003). Segmentation of objects based upon user-defined constraints is also an effective automation tool for fluorescence datasets (Raman *et al.*, 2007). The neuronal identification protocol described below incorporates some of these ideas in generating a fast and versatile approach to nerve cell identification within defined neural systems. The programs used, along with a readme file, are freely available at http://www.ece.neu.edu/groups/biomed/kamali_software.

Confocal datasets

Automated procedures were developed for identifying neurons in confocal image stacks acquired from the brainstem of larval zebrafish. Figure 1 shows a lateral view of a larva along

with the relative location of labelled brainstem neurons from a vertical perspective. Larvae were anaesthetized, rolled onto their back, embedded in agar and viewed through their dorsal surface (the optimal viewing angle for reticulospinal neurons) using an inverted fluorescence microscope (Westerfield, 1995;O'Malley & Fetcho, 2000). Confocal datasets were acquired using a BioRad MRC600 confocal imaging system (Hercules, CA, USA) with a Zeiss inverted microscope stand (Thornwood, NY, USA). In these experiments, variable subsets of the 300 known descending neurons were retrogradely labelled by injecting a fluorescent tracer into the spinal cord (see, e.g. O'Malley *et al.*, 1996;Fetcho *et al.*, 1998). The tracer then travels retrogradely up the spinal axons and into the brainstem where we see varied populations of labelled neuronal cell bodies. This labelling approach identifies these as descending neurons, i.e. neurons that project into spinal cord. Collectively, the entire set of descending neurons constitutes the Descending Motor Control System (DMCS). In a variant 'labelled-lesion' experiment, brainstem neurons are axotomized in rostral spinal cord, which leads to their fluorescent labelling in brainstem (Gahtan & O'Malley, 2001), while also producing an assortment of behavioural deficits mimicking spinal cord injury (Day *et al.*, 2005). The primary goal of the algorithms described here is to automatically recognize the labelled-lesioned neurons and to assign them to specific zones in the brainstem. This would allow higher-throughput processing of these and perhaps other neuronal datasets (such as those in Niell & Smith, 2005;Orger *et al.*, 2008).

Although images are acquired at relatively high magnification (40×), longer-working distance objectives are necessitated by the need to focus through the roughly 300 μm thickness of the intact larval brain. For most datasets a 40×, 0.75 NA water-immersion objective was used. Inherently variable aspects of both the labelling procedure and the experimental preparation lead to inconsistent image quality which poses varying degrees of challenge for automated cell segmentation and identification (Tanaka *et al.*, 2001; Pratt & Adams, 2007). Also, due to the limited field of view at this magnification, we usually acquire multiple *z*-stacks in order to span the labelled regions of the brainstem. Higher-magnification *z*-stacks (using the BioRad MRC 600's optical-zoom feature) are also acquired from regions of interest when there are many closely packed cells that we need to resolve. The data used for developing and testing our algorithms came from 11 different anaesthetized larval zebrafish and included 50 confocal image stacks or '*z*-stacks' in total. The algorithms described below seek to automate both the *detection* of neurons present in our confocal datasets and the *assignment* of each neuron to a small brainstem zone that is usually comprised of just one or two defined cell types. These algorithms depend upon the one-time construction of a brainstem template, which we describe in the next section.

Construction of a template encoding the larval DMCS

An example confocal, labelled-lesion dataset is shown in Fig. 2. The lesion is illustrated as a montage of MIPs of three confocal *z*-stacks (Fig. 2A). There are approximately 200 neurons labelled in this particular larva, but in other instances, far fewer neurons may be labelled. To illustrate the 3D distribution of neurons in this dataset, we show in Fig. 2B four individual slices from the middle image stack (which overlaps the rostral and caudal stacks, as indicated by the dotted line). The prominent Mauthner cells (asterisks) are identified in several sections as well as in the MIP montage. Other neurons can be located relative to the Mauthner neurons and to the larval midline (Fig. 2A, dashed line) which separates right and left brainstem. Additional morphological features are used for manual cell identification including cell size, somal shape, axonal trajectory and dendritic form (Kimmel *et al.*, 1982). The first step in creating a template for automated identification was to register the location of our manually identified neurons in relation to a set of landmarks in a working template. An example identification scheme for one confocal image stack is shown in Fig. 3A where different identified neurons are hand-coded by different colours. If we had larval zebrafish in which all

300 of the known descending neurons were labelled, we could directly construct a template accounting for every single neuron, but due to the stochastic nature of labelling, there are no such confocal datasets. We instead used a collection of confocal datasets to construct a template that included all known reticulospinal neurons and that would allow automatically detected neurons to be assigned to a geometrically organized set of brainstem zones.

We repeated the manual identification and colour coding shown in Fig. 3A for all confocal image stacks acquired from 11 different larval zebrafish. By transforming the collected data into a working template it was possible to establish a set of zone boundaries into which a large fraction of the manually identified neurons should correctly fall. This is illustrated in Fig. 3B as a projection of the accumulated data. To construct this projection, each larva was encoded in Adobe Photoshop as a separate layer with each neuron represented as a rectangle at its observed location in the transformed space. The neurons were colour coded as in Fig. 3A and in the projection of the 11 annotated MIP images, the colour intensity represents the density of the corresponding cell type at that location in the collected dataset (see Fig. 3 legend for further details). This provided the basis for creating a template in which the entire brainstem is divided into a series of ‘zones’ and ‘sub-zones’. The agreement of this transformation and zone identification with the original manual identification is indicated by the relatively few instances of coloured neurons falling outside of their appropriate colour zone. Note for example the few ‘orange’ RoL2/R2 cells that are not in their correct row (row #2), but are instead displaced into the top row (which contains rhombomere 1 cells such as RoL1 and RoR1). Given the relatively few errors, this provides a fairly reliable means for identifying reticulospinal neurons, thus forming the basis for constructing the DMCS template.

The DMCS template (Fig. 4) represents, in a single plane, ~260 of the 300 neurons known to descend from the larval zebrafish brain into the spinal cord (a lateral and functionally distinct group of vestibulospinal neurons is not included in the template). This template was patterned after a graphical representation of these neurons (O’Malley *et al.*, 2003), which was itself based upon much earlier work by Kimmel and coworkers (Kimmel *et al.*, 1982,1985;Metcalfe *et al.*, 1986). Each square represents a single nerve cell that is either individually identified (e.g. cells MeLm and MeLr in the top right region of the template) or that belongs to a small discrete cluster or array of neurons (as, e.g. the two MeLc cells in the same part of the template). Based on the procedure described above, the DMCS template has been organized into 28 zones – 14 on each side of the brainstem. Each zone is surrounded by a solid line and incorporates some combination of individually identified nerve cells and/or clusters of nerve cells. For example, going down to the sixth row in the template, two zones are highlighted in red. The outer zone contains just two identified cells, MiD2cm and MiD2cl. The inner zone in this row is further divided (by dashed lines) into two sub-zones. The rostral sub-zone includes two distinct cells, whereas the caudal sub-zone includes a cluster of five MiV2 cells. In some instances cells and clusters overlap in the *z*-dimension of the brainstem but for display purposes they are shown side by side in a 2D arrangement. This completes the construction of the template that we will use for our subsequent analyses of the DMCS. Note that template construction must be done just once for each distinct neural system that is to be analysed.

Image processing

With the DMCS template completed, we proceed to a three-step process in which neurons are detected and assigned to specific zones within the DMCS template. After an initial user-assisted image registration step, the remainder of the algorithm is fully automated. The three distinct stages of our processing pipeline are: (1) image registration, (2) neuronal segmentation and (3) cell assignment. In the image registration step a MIP of the confocal image stack is transformed into a normalized space. In the second stage we attempt to find the boundary locations of all neurons within this normalized space. Finally, in the last stage, we use each neuron’s relative

location to assign it to a specific zone/sub-zone of the template. This assignment is then presented to the user as a representation of the entire confocal dataset. The goal in this particular implementation is to facilitate the user's investigations into how these neuronal populations contribute to zebrafish locomotor behaviours.

Step 1: Image Registration—To register confocal *z*-stacks into a normalized space we start with a MIP projection of each confocal *z*-stack. The operator uses the computer mouse to identify pairs of corresponding points in the DMCS template and in the MIP image of the *z*-stack that is to be processed (shown as green circles with cross-hairs in Fig. 5A and B). Three such pairs of corresponding points are identified for each *z*-stack to be transformed (points are numbered 1–3 in A and B). Using an affine transform (Brown, 1992), we perform a global image transformation (Fig. 5C). Although in theory any three arbitrary pair of matched points can be used for registration, we consistently tried to identify pairs of points on the boundary between the neighbouring regions, which appear as distinct dark areas in the MIP projections as in the example illustrated. These were found to provide good loci for directing the transformation. After transforming the image stacks to template coordinates, we proceeded to the cell-segmentation step.

Step 2: Segmentation of Neurons within Confocal Image Stacks—Since spatial resolution is much higher in the transverse plane than in the *z*-direction, we apply a two-step algorithm to find neurons in image planes after transformation of the image stacks into the normalized template space. We first perform a 2D segmentation of each *xy*-plane image to find a set of intensity contours with appropriate size and shape so as to reveal each neuronal cell body present in the plane. Since a given neuron will normally be present in several images in the confocal image stack (i.e. along the optical or *z*-axis), the next step in this algorithm processes the identified contour sets in the *z*-direction to associate contours belonging to the same neuron.

The basic assumption behind our *ad hoc* 2D segmentation is that neurons can be distinguished from background and other objects such as axons and dendrites by a combination of intensity and shape thresholds. We started by simply contouring a given intensity image with a sufficiently small step between contours such that each neuron present in that image would be represented by a set of approximately concentric contours. We then applied a series of shape-thresholding criteria (based upon empirically determined parameters from our experimental datasets) to each individual contour, as follows:

1. The area of the contour should be greater than 50 pixels in the normalized space (which equates to an area of 3.1 μm^2 at the magnification used).
2. The ratio of the area of each contour to the area of the enclosing rectangle should be greater than 0.6 dimensionless units.
3. The aspect ratio of the enclosing rectangle should be greater than 0.7.
4. The ratio of the area of the contour to its perimeter should be greater than 2.2 μm.
5. A fifth criterion, which is not applied until the 3D cross-plane association step below, is that a segmented object must be present in at least two adjacent optical sections to be counted as a neuron.

The most difficult problem in this step was to find the boundary between adjacent or close-to-adjacent neurons, as neurons may appear to 'touch' one another due to diffraction, crowding in the *xy*-plane and/or overlap in the *z*-dimension. An example of this problem is shown in Fig. 6A. We addressed this apparent 'merging' of neurons by examining the locations of contour centres as we lowered the contour intensity value (Fig. 6B). Our hypothesis was that when we have adjacent neurons, the contours for each will be separate for higher contour intensities but

will merge at lower contour values, and that this merging will cause a relatively large and sudden shift in the location of the contour centre. Thus, once we identified such shifts (defined in our algorithm as a change of more than 0.8 μm over a contour level intensity change of 4 pixel intensity units), we backed up one contour level and defined the pre-merged contours as the 'boundary contours' of the neurons to which they belong. Figure 6(B) and (C) illustrate this procedure by showing unmerged contours at higher pixel intensity levels (contours 1 through 4), which merge together as the intensity level is lowered (contour 5), producing a large shift in 'd', the centroid of the contour. Identifying the lowest intensity unmerged contours, i.e. the cell boundary contours is important, as they are the basis for the subsequent cell assignment steps (see below). In the case of neurons that are well separated from one another, when we lower the contour intensity values below a certain level, a sudden shift in the location of the contour centre will occur when the neuron's contour merges into the background. In this case the boundary contour was taken as the cell's contour at the immediately higher intensity step.

Cross-plane association: Once we identified the boundary contours for all neurons in each image, we pruned all contours of lower fluorescent intensity than the identified boundary contours and proceeded to the cross-plane association problem. Here our basic assumption was that centres of contour sets of the same neuron in adjacent slices should be close to lying on a line which was itself close to parallel to the optical axis. To find these collinear points, we again applied an *ad hoc* algorithm, this one based on the Hough transform (Ballard, 1987; Gonzalez & Woods, 1987; Gonzalez *et al.*, 2004). The Hough transform, as used here, finds points in a plane, which lie approximately along the same line by parameterizing the line and then mapping each candidate point to a line in the parameter space. Sets of points which all lie on or near the same line will correspond to lines which are mutually intersecting or are close to intersecting in parameter space.

To apply this approach, we first transformed all retained contours (including boundary and internal contours) in the entire *z*-stack into a new 3D space. In this transformation, the centre of each contour was defined as the centre of a bounding rectangle oriented along the *x*- and *y*-axes. The third coordinate in this new space, *Z*, is defined as:

$$Z = M\left(z + \frac{i}{255}\right)$$

where *i* denotes the contour intensity value, *z* is the index of the *z*-stack slice that the contour belongs to, and *M* is a fixed number that adjusts the resolution along the new *z*-axis. Thus the 'stack of contours' shown in Fig. 6 will occupy an interval in the *z*-dimension that is above that occupied by any contours of the same neuron in a lower image plane, and below any contours of that neuron in the image plane above. In order to detect lines in this space, we projected the centres of all contours in a given *z*-stack onto the *yz* and *xz* planes. We used the 2D Hough transform in both projections to associate centres belonging to the same neuron, and then 'back-projected' these associations into 3D space to associate the contours as well as the centres. The end result of this implementation of the Hough transform was to link all contours from a single neuron across the *z*-planes. In the final cell assignment step, the outermost boundary contours of a cell, occurring in different *z*-planes but associated with each other, are used collectively to assign each cell to a specific location within the brainstem.

Step 3: Cell Identification – Assignment of Neurons to Zones and Sub-Zones: The template described earlier was used in conjunction with the segmented boundary contours to assign detected neurons to specific zones and sub-zones of the brainstem. The assignment algorithm had two steps: (1) Associate the identified 3D neurons with the proper zones and (2) when

applicable, associate neurons with the proper sub-zones within a zone. As noted earlier, sub-zones are found in regions where groupings of neurons tend to overlap to some extent in an *xy* projection, but can be differentiated in part based upon their medial-lateral location or their distribution along the dorsal-ventral (*z*-)axis. We describe here our assignment procedure for both the sub-divided and undivided zones.

Zone assignments: We used a simple rule to assign each segmented neuron to a particular zone. An individual boundary contour was assigned to a zone if its area had more than 70% overlap with a zone; otherwise it was labelled as unresolved. Given a set of boundary contours for a neuron along the *z*-axis, we calculated the fraction that was associated to a particular zone. If more than half of a cell's boundary contours belonged to a specific zone, then it was assigned to that zone; otherwise it was marked as unresolved.

Sub-divided zones: For zones comprised of sub-zones, the neuron was further categorized by attempting to assign it to one of the two sub-zones. One of two rules was applied:

1. Some zones were subdivided based upon dorsal-ventral location, i.e. based on their *z*-location within the *z*-stack. For these zones, neurons were assigned to either the dorsal or ventral sub-zone, depending upon which sub-zone contained more of the cell's boundary contours.
2. Other zones were subdivided in the *xy* plane along the medial-lateral axis. In this case we calculated the Euclidean distance between the centroid of the neurons in the zone and the brainstem midline and then assigned the neuron to the sub-zone in which its centroid lay.

Results

To evaluate the utility of the cell-segmentation and cell-identification algorithms, we subjected our experimental confocal dataset to a number of tests. Figure 7 illustrates a comparison between our contour-based segmentation and a simple implementation of a popular watershed segmentation algorithm (Beucher, 1992; and see Vincent & Soille, 1991). The raw dataset (Fig. 7A) contains a number of neurons in close proximity. With the watershed algorithm (Fig. 7B), there can be an over-segmentation effect in which individual neurons are broken into multiple pieces, as shown for neuron #29 (enclosed within a red box in all three panels), which has been broken down into 3 pieces. Such over-segmentation was common with our datasets. By contrast, our boundary contour method (described above) provided a more accurate means of detecting and segmenting neurons (Fig. 7C), in terms of agreement with the ground truth data as described below.

Figure 8 shows representative optical sections from three different zebrafish that illustrate the algorithm's ability to segment neuronal structures at different brainstem locations. The automated segmentation results are illustrated by the grey contours surrounding the neurons. Quite often in these *in vivo* datasets, the fluorescence signals from cells are overlapping – both in the *z*-dimension and in the *xy*-plane – depending upon such factors as actual cell proximity, the intensity of the fluorescence signal, diffraction, light scattering and instrument settings. In such instances where cells have contours that are initially 'touching' in the confocal section, they have been resolved or segmented based upon the boundary contour procedure described above; four such instances of segmented 'touching' cell pairs (outlined in the red boxes) are shown in Fig. 8.

Quantitative performance of the algorithms

The ability of our algorithms to correctly detect and identify neurons is quantified in the next two tables. To evaluate the performance of these protocols, we compared the algorithm's output with our prior ground-truth manual identification of these brainstem neurons. One caveat is that this 'ground truth' identification by experts is not absolute, given such factors as image quality and the complexity of the datasets. Although we currently consider manual identification to rank highest in reliability, we should consider that algorithmic analysis may enhance or improve upon manual identification. Table 1 summarizes the output of the cell-segmentation and cell-identification components of this protocol.

The efficacy of cell segmentation was assessed by comparing the algorithm's output with the manual identification of neurons throughout a set of *z*-stacks encompassing the brainstem of 11 different zebrafish. Table 1 shows that the number of manually recognized neurons agrees fairly well with the number of neurons detected by the algorithm (# segmented). The agreement is best reflected by those neurons recognized in common by both methods – the 'correctly segmented' neurons. The instances where the manual and automated methods diverge fall into two categories. First, there are instances where the algorithm identified objects as neurons that were not so identified manually – nominally 'false positives'. Secondly, there are 'false negatives' – instances where the algorithm missed objects that were manually recognized as neurons. Although there were modest numbers of 'errors' in both categories, it should be noted that this is a real-world dataset of 11 larvae that were chosen for experimental analysis (i.e. that had sufficient neuronal labelling to warrant behavioural evaluation). Some of the datasets were of poor optical quality, as e.g. *Fish 203*, where only 10 of 19 manually identified neurons were recognized by the algorithm. But in the remainder of this database, the number of neurons that were correctly segmented by the algorithm ranged from 67% to 100%, with a database-wide agreement for segmentation of 454 of the 537 manually identified neurons or 84.5%. This is sufficient to substantially speed up our labelled-lesion project.

For this same dataset, Table 1 also shows the number of neurons (taken from just the correctly segmented neurons) that were 'unresolved' in that they did not meet criterion for inclusion in a zone. Only a very small fraction of the correctly segmented neurons were not assigned to zones. The final column shows a slightly larger number of instances in which neurons were resolved but assigned to an incorrect zone. Overall, if we subtract both the unresolved and mis-assigned neurons from those neurons that were correctly segmented, this leaves 436 of 537 neurons assigned to their correct zone – that is 81.2% of the entire population of manually identified neurons was correctly identified by the algorithm. Although improvements in the cell segmentation and identification steps would be desirable, the structures found or missed were not obvious errors, but instead reflect difficulties encountered in both the manual and automated procedures.

In our semi-automatic registration process, we use a graphical user interface to register points between the MIP image and the DMCS template, by simply clicking on corresponding points with a computer mouse (Fig. 5). One issue is the precision with which these points can be selected and whether or not the algorithm is sensitive to small displacements of the selected points. Our preferred approach was to pick one pair of corresponding points on the mid-line and two other pairs on any two zone borders that were easily recognized and were symmetrical with respect to the mid-line. This method turned out to be reasonably robust to small displacements of the registration points. In about one-third of the datasets, however, selecting such a set of symmetrical, corresponding points was not straightforward. For instance, some *z*-stacks did not contain symmetrical neuron pairs or neuronal clusters to help find zone boundaries, whereas others had only unilateral labelling. In such situations we repetitively registered each *z*-stack (up to three or four times), selecting different sets of corresponding points each time, and then for each such candidate registration, proceeded with the rest of the

zonal identification algorithm. We obtained essentially identical results with the different registration points, indicating a relatively robust classification protocol – within the context of the generally good agreement between the algorithm's results and the manual-identification results.

Unseen datasets

We also examined the ability of our template to classify neurons in previously 'unseen' datasets by employing a 'leave-one-out' test, as follows: using our collection of confocal image stacks from 11 zebrafish, we cyclically left out the *z*-stacks from one of the 11 fish and used the other 10 datasets to build a new template. We then used each new template to assign neurons that were segmented from the 'left-out' *z*-stack. Table 2 presents the results of this leave-one-out test in terms of cell identification (zone assignment) accuracy; note that the unresolved neurons were excluded from this analysis. For the correctly segmented neurons, the algorithm was highly effective in assigning neurons from unseen datasets to their correct zones in the leave-one-out templates: of the 11 trials on unseen datasets, 10 resulted in assignments identical to those obtained using the template constructed from the complete dataset. The only exception was *Fish 200* in which one neuron was mis-assigned in the leave-one-out procedure, whereas all 58 resolved neurons were correctly assigned when using the whole-dataset template (compare results for *Fish 200* in Tables 1 and 2). This result shows that templates constructed from a 'training dataset' can effectively identify neurons in new brainstem datasets, an approach that should in principle be applicable to other neural structures.

Presentation of results

The results of this cell identification protocol can be provided to users in a variety of forms. One option is to display all segmented neurons along with a cell identification code. In Fig. 9, three example sections from an image stack are shown in which each boundary contour or neuron is given a unique identifying number (which remains the same across planes for that neuron). The specific cell type (or cluster type) is indicated by the accompanying colour key. In some instances the assignment is to a zone containing several cell types, such as the zone containing the purple MiR1-MiM1 cell types. Providing each cell's location with respect to other labelled cells and landmarks allows users to perform further classification within a zone – e.g. distinguishing the purple cells #55 and #52 as either MiR1 or MiM1. Because the display merges the optical sections and boundary contours, it also enables easy review of instances where the algorithm and manual identification diverge. By viewing the boundary contours of false positives (objects recognized only by the algorithm) the user can decide whether or not to accept these objects' identification. Similarly, 'neurons' not given boundary contours (false negatives) can be manually assigned identities and added to the collected record. Automated classification is valuable in sparsely labelled larval zebrafish, where there may be few nearby landmarks, and becomes more valuable when there are many dozens or hundreds of labelled cells because manual identification in those situations is tedious and uncertain. The algorithm further helps the investigator by resolving merged fluorescence structures into individual neurons. Although further automation might refine cell identification, the current program accomplishes most of the desired classification by virtue of its segmentation and zone assignment algorithms.

The morphometric data collected can be visualized by a variety of means. Figure 10 shows a segmented, 3D dataset that has been projected from three different views, using a volume rendering feature in the free SciRun/BioPSE software package (reviewed by Bitter *et al.*, 2007). Stacks of boundary contours are shown in the context of a 3D representation of the brainstem dataset. A reference set of coordinate axes is shown in the upper right of both panels. The blue arrow indicates the orientation of the *z*-axis of the dataset, which is roughly parallel to the dorsal-ventral axis of the fish. The red arrow indicates the longitudinal (rostral-caudal)

axis of the brainstem, whereas the green arrow represents the medial-lateral axis. The locations of the neuronal boundary contours generated by the segmentation algorithm are superimposed as solid black lines on the volume-rendered image, providing a 3D view of the algorithm's overall output.

The morphological measurements and other data generated can be used in further ways. For example, data from an image stack containing eight MeL cells has been auto-quantified and displayed in tabular form (Table 3). Although details such as cell position and size can aid cell identification efforts, they may also benefit other kinds of systematic analyses that incorporate, e.g. physiological or molecular data. The morphometric data obtained here is intended to serve as an input to our labelled-lesion experiments in which the makeup of lesioned neuronal populations is related to specific behavioural deficits (Gahtan & O'Malley, 2001;Day *et al.*, 2005). In this instance, enhanced quantification of morphometric data may facilitate potentially finer-grained identification of neurons within the 10 ostensibly 'homogeneous' clusters and arrays of cells present in our template (Fig. 4). An ultimate goal is for the algorithms provided here to contribute to a NeuronBank-like database, such as that created for individually identified invertebrate neurons (Calin-Jageman *et al.*, 2007).

Discussion

Cell identification protocols have been used in certain domains (Conrad *et al.*, 2004; Chen *et al.*, 2006), but the methods provided here are, to our knowledge, the first to recognize individually identified neurons in 3D confocal datasets. Although a variety of segmentation and processing algorithms might be employed to locate nerve cells in confocal image stacks, the relatively simple and fast protocol described here proved effective for identifying reticulospinal neurons in living zebrafish. One limitation is that when neural datasets are acquired from living animals or brain slices, imaging conditions are rarely ideal because of light scattering. Image degradation occurs with conventional fluorescence microscopy, as well as confocal and two-photon imaging, and generally worsens with increasing depth into the specimen. Nonetheless, automated analysis of confocal datasets spanning the thickness of the *in vivo* larval brain (approximately 300 μm thick) yielded better than 80% identification of neurons – thus providing a favourable test of a protocol that is potentially applicable to other neuronal and confocal datasets.

Within the DMCS template there are, if we add undivided zones and sub-zones together, a total of 20 discrete sections in the template (duplicated on each side of the brainstem). Of the 20 sections, 10 have but a single specified cell type that ranges in number from 1 to 12 neurons (Fig. 4). Automated assignment to such sections thus provides an 'exact' identification (or as exact as manual identification achieves). Of the remaining sections, six have just two cell types. Thus for a large majority of zones, successful cell assignment results in immediate and relatively precise identification of cells throughout the brainstem. The user may wish to further resolve cell identities, based on additional cell features, and may also wish to compare the raw dataset with the algorithmic results to evaluate nominal false negatives and positives. In our experience, the pure manual procedure was so time consuming (and tedious) that the automation could save 2 h or more for each confocal image stack analysed, even with manual scanning of the algorithm's results (Fig. 9). The algorithm runs in about 2 min per image stack on a typical desktop computer. With an average of about five image stacks per fish, this suggests a savings of around 10 h per typical experiment. The time savings is greatest for larger datasets that may contain hundreds of labelled neurons. This tool will thus allow us to analyse many more datasets than was previously possible – while gaining complementary and potentially enhanced information.

To summarize our protocol, confocal datasets are processed in three sequential steps: image registration, segmentation and cell assignment. Beyond the initial selection of three registration points (which in the worse cases needs to be repeated three or four times), the program is fully automatic, and none of its parameters need to be adjusted by the user in this implementation. The protocol was designed to be fast and appropriate for the data and purpose at hand. Because the three steps are carried out independently, each step might easily be replaced by an alternative method (see, e.g. Cseke, 1992; Tanaka *et al.*, 2001; Ruggeri & Pajaro, 2002; Chen *et al.*, 2006). This provides flexibility to modify the algorithm to enhance its resolution or to tailor it for other kinds of neuronal datasets. For example, any 3D algorithm that is reasonably fast and accurate and which provides boundary contours could be used for the segmentation step. One might also improve the detection of neurons by incorporating additional discrimination features and extending them into the *z*-dimension. This could include such features as 3D shape, volume and dendritic/axonal morphologies. With regard to the classification zones, rectangular 2D regions were used because they were convenient and adequate for the geometries of our experimental preparation, but other regional classification schemes could as easily be used. Although changes in performance of one step in the algorithm might affect overall program performance, the steps are largely independent, and so it should be possible to directly evaluate the consequences of trial modifications.

There are many methods for analysing neuroanatomical datasets. For example, stereological methods are used to quantify large numbers of nerve cells and synapses (Popken & Farel, 1997; Geuna, 2000, [2005]; Kubinova & Janacek, 2001; Ma *et al.*, 2003). Most stereological methods, however, are not automated, nor are they used to assign neurons to specific functional classes. Other automated methods include image registration and structure tracing through 3D datasets (Al-Kofahi *et al.*, 2003a, b, 2006; Barber *et al.*, 2003), but again they are not used for cell-identification purposes. The algorithms provided here automatically identify neurons with a precision roughly similar to that of expert users. The modest number of discrepancies might be viewed as ‘algorithm errors’ (i.e. false positives or false negatives, as designated), but it is at present uncertain as to which method, manual or automated, is actually better at detecting bona fide nerve cell bodies and determining their identity. Further research, into these objects’ anatomical and phenotypic features would be needed to more conclusively compare manual vs. algorithmic performance. Eventually, automation may offer superior performance in classification while also helping tie data from diverse sources into a common, template-driven framework –an objective currently being pursued in invertebrate nervous systems (Calin-Jageman *et al.*, 2007) and, in a more general sense, in vertebrate animals (Dyhrfjeld-Johnsen *et al.*, 2005; Bota & Swanson, 2007; Martone *et al.*, 2008).

The extent to which our algorithms can be applied to other neural systems has not been evaluated. The biggest hurdle is probably the construction of a system-specific cell-identification template. But this only needs to be done once for each system, and in our case the time investment was small in comparison to the time already invested in manual identification of neurons in the zebrafish confocal datasets. Since most neural architectures are investigated in parallel by multiple research groups, the creation of such system-specific templates should be a modest investment in relation to the rapidly accumulating quantities of phenotypic data. In cases where suitable landmarks can be recognized, and annotated 3D datasets are available to create a valid template, it should be possible to generate an effective identification protocol. In our case, we were aided by the relative ease with which the image stacks can be oriented and aligned (step 1), using e.g. the paired Mauthner cells. Neuronal identification (step 3) also depends upon the efficacy of the cell-segmentation algorithm (step 2) and so it may be necessary to modify the cell-inclusion criteria and/or other components of the algorithmic sequence in order to achieve good identification results.

We expect that efforts to codify cell identity in a variety of neural architectures could prove useful – especially in systems with many distinct nerve cell types that are anatomically intermingled. Emerging technologies in the areas of genetic tagging and manipulation (Luo *et al.*, 2008) should prove highly synergistic with automated cell-identification protocols. In zebrafish, a Gal4 enhancer trap enables the genetic tagging of phenotypically related neurons (Scott *et al.*, 2007) as well as genetic inactivation using, e.g. a tetanus toxin light chain (Asakawa *et al.*, 2008). Optical-control proteins, such as channel-rhodopsin (Zhang *et al.*, 2006; Huber *et al.*, 2008) and light-activated glutamate receptors (Szobota *et al.*, 2007), could in principle be targeted in this manner. Such approaches would benefit from having the identities of the fluorescently labelled neurons analysed in a quantitative and automated fashion. Thus, our goal for this technology is not just to accelerate data throughput, but to improve upon current cell-identification techniques.

In the case of the larval zebrafish DMCS, we currently recognize 40 distinct descending cell types based upon anatomical features including brainstem location, but future experiments may subdivide this population (which has 150 neurons in total on each side of brainstem) and thereby increase the number of individually identifiable cell types. Alternatively, a minimalist classification scheme might lump together some of the 40 known (i.e. user-defined) DMCS cell types, thus 'reducing cell diversity' and, as such, the identification problem. Intracellular fills of these cells, however, have revealed extreme diversity in their axonal projection patterns in spinal cord, indicating that they are both individually recognizable and functionally distinct. This was true even for three escape-eliciting neurons that were believed to form a single functional class (Gahtan & O'Malley, 2003). There is likely to be equivalent or greater local-circuit diversity and complexity in most other parts of the vertebrate brain including the retina (MacNeil & Masland, 1998), cerebral cortex (Tseng & Prince, 1993; Stevens, 1998), hippocampus (Jinno *et al.*, 2007) and optic tectum (Baez *et al.*, 2003; Niell & Smith, 2005). Automation of image analysis in such systems should lead to a more precise and reproducible quantification of each system's neuronal constituents. The absence of such an accounting could be likened to the situation of an auto mechanic trying to fix a car without knowing all of the functional parts, or even how many parts there should be. For us 'neuromechanics', we expect that advances in neuronal classification, in conjunction with automated image analysis, will facilitate efforts to understand and repair diverse neural systems.

Acknowledgments

We thank Eric Miller for his helpful comments in the early stages of this work and David Weinstein for his assistance with the SciRun visualization of segmentation results. We also thank two anonymous reviewers for helpful suggestions. The work of M.K. and D.B. was supported in part by the Center for Integrative Biomedical Computing, National Institutes of Health, National Center for Research Resources under Grant 1-P41-RR12553–7. Support for our confocal facility was provided by NU's Gordon Center for Subsurface Sensing and Imaging Systems.

References

Al-Kofahi KA, Can A, Lasek S, et al. Median-based robust algorithms for tracing neurons from noisy confocal microscope images. IEEE Trans Info Technol Biomed 2003a;7:302–317.

Al-Kofahi O, Can A, Lasek S, Szarowski DH, Turner JN, Roysam B. Algorithms for accurate 3D registration of neuronal images acquired by confocal scanning laser microscopy. J Microsc 2003b; 211:8–18. [PubMed: 12839546]

Al-Kofahi O, Radke RJ, Roysam B, Banker G. Automated semantic analysis of changes in image sequences of neurons in culture. IEEE Trans Biomed Eng 2006;53:1109–1123. [PubMed: 16761838]

Asakawa K, Suster ML, Mizusawa K, et al. Genetic dissection of neural circuits by Tol2 transposon-mediated Gal4 gene and enhancer trapping in zebrafish. Proc Natl Acad Sci USA 2008;105:1255–1260. [PubMed: 18202183]

Baez J, Monzon-Mayor M, Yanes C, del Mar Romero-Aleman M, Francisco Arbelo-Galvan J, Puelles L. Neuronal differentiation patterns in the optic tectum of the lizard Gallotia galloti. Brain Res 2003;975:48–65. [PubMed: 12763592]

Barber PR, Vojnovic B, Ameer-Beg SM, Hodgkiss RJ, Tozer GM, Wilson J. Semi-automated software for the three-dimensional delineation of complex vascular networks. J Microscopy 2003;211:54–62.

Benito-Gutiérrez È. A gene catalogue of the amphioxus nervous system. Int J Biol Sci 2006;2:149–160. [PubMed: 16763675]

Bernhardt RR, Chitnis AB, Lindamer L, Kuwada JY. Identification of spinal neurons in the embryonic and larval zebrafish. J Comp Neurol 1990;302:603–616. [PubMed: 1702120]

Beucher S. The watershed transformation applied to image segmentation. Scanning Microsc Inter 1992;6:299–314.

Bitter I, Van Uitert R, Wolf I, Ibáñez L, Kuhnigk JM. Comparison of four freely available frameworks for image processing and visualization that use ITK. IEEE Trans Vis Comput Graph 2007;13:483–493. [PubMed: 17356215]

Bota M, Swanson LW. The neuron classification problem. Brain Res Rev 2007;56:79–88. [PubMed: 17582506]

Bota M, Dong HW, Swanson LW. Brain architecture management system. Neuroinformatics 2005;3:15–48. [PubMed: 15897615]

Boyan G, Therianos S, Williams JL, Reichert H. Axogenesis in the embryonic brain of the grasshopper Schistocerca gregaria: an identified cell analysis of early brain development. Development 1995;121:75–86. [PubMed: 7867509]

Broit, C. PhD Thesis. University of Pennsylvania; 1981. Optimal registration of deformed images.

Brown LG. A survey of image registration techniques. ACM Comput Surv 1992;24:325–376.

Buchanan JT. Contributions of identifiable neurons and neuron classes to lamprey vertebrate neurobiology. Prog Neurobiol 2001;63:441–466. [PubMed: 11163686]

Calin-Jageman, RJ.; Dhawan, A.; Yang, H., et al. Development of NeuronBank: a federation of customizable knowledge bases of neuronal circuitry. Proceedings of the 1st IEEE International Workshop on Service Oriented Technologies for Biological Databases and Tools – IEEE Services Computing Workshops (SOBDAT/SCW 2007); July 13; Salt Lake City, Utah. 2007. p. 114-121.

Cazalets JR, Nagy F, Moulins M. Suppressive control of the crustacean pyloric network by a pair of identified interneurons. I Modulation of the motor pattern. J Neuro 1990;10:448–457.

Chen X, Zhou X, Wong STC. Automated segmentation, classification, and tracking of cancer cell nuclei in time-lapse microscopy. IEEE Trans Biomed Eng 2006;53:762–766. [PubMed: 16602586]

Christensen GE, Rabbitt RD, Miller MI. 3D brain mapping using a deformable neuroanatomy. Phys Med Biol 1994;39:609418.

Conrad C, Erfle H, Warnat P, et al. Automatic identification of subcellular phenotypes on human cell arrays. Genome Research 2004;14:1130–1136. [PubMed: 15173118]

Cseke, I. A fast segmentation scheme for white blood cell images. Pattern Recognition: Image, Speech and Signal Analysis, Proceedings 11th IAPR International Conference; The Hague; 1992. p. 530-533.

Davatzikos C, Prince JL, Bryan RN. Image registration based on boundary mapping. IEEE Trans Med Imaging 1996;15:112–115. [PubMed: 18215894]

Davis GR Jr, McClellan AD. Long distance axonal regeneration of identified lamprey reticulospinal neurons. Exp Neurol 1994;127:94–105. [PubMed: 7515355]

Day LJ, Knudsen DP, Dhanota H, Severi K, Jose JV, O'Malley DM. Lesions of descending motor pathways deconstrain spinal activity patterns: results from larval zebrafish. Soc Neurosci Abs 2005 2005:#751.11.

De Felipe J. Neocortical neuronal diversity: chemical heterogeneity revealed by colocalization studies of classic neurotransmitters, neuropeptides, calcium-binding proteins, and cell surface molecules. Cerebral Cortex 2004;3:273–289.

Deliagina TG, Zelenin PV, Orlovsky GN. Encoding and decoding of reticulospinal commands. Brain Res Rev 2002;40:166–177. [PubMed: 12589915]

Drapeau P, Ali DW, Buss RR, Saint-Amant L. In vivo recording from identifiable neurons of the locomotor network in the developing zebrafish. J Neurosci Meth 1999;88:1–13.

Dyhrfjeld-Johnsen J, Maier J, Schubert D, Staiger J, Luhmann HJ, Stephan KE, Kötter R. CoCoDat: a database system for organizing and selecting quantitative data on single neurons and neuronal microcircuitry. J Neurosci Meth 2005;141:291–308.

Eaton RC, Farley RD. Mauthner neuron field potential in newly hatched larvae of the zebra fish. J Neurophys 1975;38:502–512.

Eaton RC, Lee RK, Foreman MB. The Mauthner cell and other identified neurons of the brainstem escape network of fish. Prog Neurobiol 2001;63:467–485. [PubMed: 11163687]

Fetcho JR, O'Malley DM. Visualization of active neural circuitry in the spinal cord of intact zebrafish. J Neurophys 1995;73:399–406.

Fetcho JR, Cox KJA, O'Malley DM. Monitoring activity in neuronal populations with single-cell resolution in a behaving vertebrate. Histochem J 1998;30:153–167. [PubMed: 10188924]

Fischl B, Salat DH, Busa E, et al. Whole brain segmentation: automated labeling of neuroanatomical structures in the human brain. Neuron 2002;33:341–355. [PubMed: 11832223]

Friedrich RW, Korsching SI. Combinatorial and chemotopic odorant coding in the zebrafish olfactory bulb visualized by optical imaging. Neuron 1997;18:737–752. [PubMed: 9182799]

Friesen WO, Poon M, Stent GS. Neuronal control of swimming in the medicinal leech. IV Identification of a network of oscillatory interneurones. J Exp Biol 1978;75:25–43. [PubMed: 702043]

Furukawa T, Furshpan EJ. Two inhibitory mechanisms in the Mauthner neurons of goldfish. J Neurophysiol 1963;26:140–176. [PubMed: 13945908]

Gahtan E, O'Malley DM. Rapid lesioning of large numbers of identified vertebrate neurons: applications in zebrafish. J Neurosci Meth 2001;108:97–110.

Gahtan E, O'Malley DM. Visually guided injection of identified reticulospinal neurons in zebrafish: a survey of spinal arborization patterns. J Comp Neurol 2003;459:186–200. [PubMed: 12640669]

Gahtan E, Sankrithi N, Campos JB, O'Malley DM. Evidence for a widespread brain stem escape network in larval zebrafish. J Neurophysiol 2002;87:608–614. [PubMed: 11784774]

Gahtan E, Tanger P, Baier H. Visual prey capture in larval zebrafish is controlled by identified reticulospinal neurons downstream of the tectum. J Neurosci 2005;25:9294–9303. [PubMed: 16207889]

Gal JS, Morozov YM, Ayoub AE, Chatterjee M, Rakic P, Haydar TF. Molecular and morphological heterogeneity of neural precursors in the mouse neocortical proliferative zones. J Neurosci 2006;26:1045–1056. [PubMed: 16421324]

Gee, JC.; Bajcsy, RK. Elastic matching: continuum mechanical and probabilistic analysis. In: Toga, AW., editor. Brain Warping. Academic Press; New York: 1998. p. 183-197.

Geuna S. Appreciating the difference between design-based and model-based sampling strategies in quantitative morphology of the nervous system. J Comp Neurol 2000;427:333–339. [PubMed: 11054696]

Geuna S. The revolution of counting "tops": two decades of the dissector principle in morphological research. Microsc Res Tech 2005;66:270–274. [PubMed: 15940681]

Gong S, Zheng C, Doughty ML, et al. A gene expression atlas of the central nervous system based on bacterial artificial chromosomes. Nature 2003;425:917–925. [PubMed: 14586460]

Gonzalez, RC.; Woods, RE. Digital image processing. Addison-Wesley; Reading, MA: 1987.

Gonzalez, RC.; Woods, RE.; Eddins, SL. Digital Image Processing using MATLAB. Prentice Hall; Upper Saddle River, NJ: 2004.

Hale ME, Ritter DA, Fetcho JR. A confocal study of spinal interneurons in living larval zebrafish. J Comp Neurol 2001;437:1–16. [PubMed: 11477593]

Herdegen T, Leah JD. Inducible and constitutive transcription factors in the mammalian nervous system: control of gene expression by Jun, Fos and Krox, and CREB/ATF proteins. Brain Res Brain Res Rev 1998;28:370–490. [PubMed: 9858769]

Hochheiser H, Yanowitz J. If I only had a brain: exploring mouse brain images in the Allen brain atlas. Biol Cell 2007;99:403–409. [PubMed: 17567264]

Howard, V.; Reed, MG. Unbiased Stereology: Three-dimensional Measurement in Microscopy. Springer; New York: 1998.

Huber D, Petreanu L, Ghitani N, Ranade S, Hromádka T, Mainen Z, Svoboda K. Sparse optical microstimulation in barrel cortex drives learned behaviour in freely moving mice. Nature 2008;451:61–64. [PubMed: 18094685]

Jinno S, Klausberger T, Marton LF, et al. Neuronal diversity in GABAergic long-range projections from the hippocampus. J Neurosci 2007;27:8790–8804. [PubMed: 17699661]

Joshi SC, Miller MI. Landmark matching via large deformation diffeomorphisms. IEEE Trans Image Process 2000;9:1357–1370. [PubMed: 18262973]

Katz PS, Harris-Warrick RM. Actions of identified neuromodulatory neurons in a simple motor system. Trends Neurosci 1990;13:367–373. [PubMed: 1699326]

Kimmel CB, Powell SL, Metcalfe WK. Brain neurons which project to the spinal cord in young larvae of the zebrafish. J Comp Neurol 1982;205:112–127. [PubMed: 7076887]

Kimmel CB, Metcalfe WK, Schabtach E. T-reticular interneurons: a class of serially repeating cells in the zebrafish hindbrain. J Comp Neurol 1985;233:365–376. [PubMed: 3980775]

Korn H, Faber DS. An electrically mediated inhibition in goldfish medulla. J Neurophysiol 1975;38:452–471. [PubMed: 1127450]

Kubinova L, Janacek J. Confocal microscopy and stereology: estimating volume, number, surface area and length by virtual test probes applied to three-dimensional images. Microsc Res Tech 2001;53:425–435. [PubMed: 11525261]

Kupfermann I, Kandel ER. Neuronal controls of a behavioral response mediated by the abdominal ganglion of Aplysia. Science 1969;164:847–850. [PubMed: 5767790]

Lewis KE, Eisen JS. From cells to circuits: development of the zebrafish spinal cord. Prog Neurobiol 2003;69:419–49. [PubMed: 12880634]

Li L. Zebrafish mutants: Behavioral genetic studies of visual system defects. Develop Dynamics 2001;221:365–372.

Liu K, Fetcho JR. Laser ablation reveals functional relationships of segmental hindbrain neurons in zebrafish. Neuron 1999;23:325–335. [PubMed: 10399938]

Luo L, Callaway EM, Svoboda K. Genetic dissection of neural circuits. Neuron 2008;57:634–660. [PubMed: 18341986]

Ma SY, Longo FM, Roytta M, Collan Y. Modern stereological evaluation in the aging human substantia nigra. Image Anal Stereol 2003;22:73–80.

Maccaferri G, Lacaille JC. Interneuron Diversity series: Hippocampal interneuron classifications – making things as simple as possible, not simpler. Trends Neurosci 2003;26:564–571. [PubMed: 14522150]

Machado AMC, Gee JC. Atlas warping for brain morphometry. SPIE 2003;3338:642.

Mackler SA, Selzer ME. Specificity of synaptic regeneration in the spinal cord of the larval sea lamprey. J Physiol 1987;388:183–198. [PubMed: 3656190]

MacNeil MA, Masland RH. Extreme diversity among amacrine cells: implications for function. Neuron 1998;20:971–982. [PubMed: 9620701]

Marmigere F, Ernfors P. Specification and connectivity of neuronal subtypes in the sensory lineage. Nat Rev Neurosci 2007;8:114–127. [PubMed: 17237804]

Martone ME, Zhang S, Gupta A, et al. The cell-centered database: a database for multiscale structural and protein localization data from light and electron microscopy. Neuroinformatics 2003;1:379–395. [PubMed: 15043222]

Martone ME, Tran J, Wong WW, et al. The cell centered database project: an update on building community resources for managing and sharing 3D imaging data. J Struct Biol 2008;161:220–331. [PubMed: 18054501]

Masland RH. Neuronal diversity in the retina. Curr Opin Neurobiol 2001;11:431–436. [PubMed: 11502388]

Metcalfe WK, Mendelson B, Kimmel CB. Segmental homologies among reticulospinal neurons in the hindbrain of the zebrafish larva. J Comp Neurol 1986;251:147–159. [PubMed: 3782495]

Nakayama H, Oda Y. Common sensory inputs and differential excitability of segmentally homologous reticulospinal neurons in the hindbrain. J Neurosci 2004;24:3199–3209. [PubMed: 15056699]

Nelson SB, Hempel C, Sugino K. Probing the transcriptome of neuronal cell types. Curr Opin Neurobiol 2006a;16:571–576. [PubMed: 16962313]

Nelson SB, Sugino K, Hempel CM. The problem of neuronal cell types: a physiological genomics approach. Trends Neurosci 2006b;29:339–345. [PubMed: 16714064]

Niell CM, Smith SJ. Functional imaging reveals rapid development of visual response properties in the zebrafish tectum. Neuron 2005;45:941–951. [PubMed: 15797554]

Okazaki M, Takeda R, Haji A, Yamazaki H. Glutamic acid decarboxylase-immunoreactivity of bulbar respiratory neurons identified by intracellular recording and labeling in rats. Brain Res 2001;914:34–47. [PubMed: 11578595]

O'Malley, DM.; Fetcho, JR. The zebrafish hindbrain: a transparent system for imaging motor circuitry. In: Yuste, R.; Lanni, F.; Konnerth, A., editors. Imaging Living Cells. Cold Spring Harbor Laboratory Press; Cold Spring Harbor, NY: 2000. p. 14.11-14.12.

O'Malley DM, Kao YH, Fetcho JR. Imaging the functional organization of zebrafish hindbrain segments. Neuron 1996;17:1145–1155. [PubMed: 8982162]

O'Malley DM, Zhou Q, Gahtan E. Probing neural circuits in the zebrafish: a suite of optical techniques. Methods 2003;30:49–63. [PubMed: 12695103]

Orger MB, Kampff AR, Severi KE, Bollmann JH, Engert F. Control of visually guided behavior by distinct populations of spinal projection neurons. Nature Neurosci 2008;11:327–333. [PubMed: 18264094]

Popken GJ, Farel PB. Sensory neuron number in neonatal and adult rats estimated by means of stereologic and profile-based methods. J Comp Neurol 1997;386:8–15. [PubMed: 9303521]

Pratt, WK.; Adams, JE, Jr. Digital Image Processing. John Wiley & Sons; Hoboken, NJ: 2007.

Raman S, Maxwell CA, Barcellos-Hoff MH, Parvin B. Geometric approach to segmentation and protein localization in cell culture assays. J Microsc 2007;225:22–30. [PubMed: 17286692]

Rovainen CM. Physiological and anatomical studies on large neurons of central nervous system of the sea lamprey (*Petromyzon marinus*). I Muller and Mauthner cells. J Neurophysiol 1967;30:1000–1023. [PubMed: 6069724]

Ruggeri A, Pajaro S. Automatic recognition of cell layers in corneal confocal microscopy images. Computer Meth Programs Biomed 2002;68:25–35.

Schulz DJ, Goaillard JM, Marder EE. Quantitative expression profiling of identified neurons reveals cell-specific constraints on highly variable levels of gene expression. Proc Natl Acad Sci 2007;104:13187–13191. [PubMed: 17652510]

Scott EK, Mason L, Arrenberg AB, et al. Targeting neural circuitry in zebrafish using GAL4 enhancer trapping. Nat Methods 2007;4:323–326. [PubMed: 17369834]

Severi KE, Orger MB, Talsania S, Kampff AR, O'Malley DM, Engert F. Diversity of visuomotor-response profiles of larval zebrafish reticulospinal neurons revealed by in vivo calcium imaging. Soc Neurosci Abstr 2007 2007:#924.9.

Shamir M, Sompolinsky H. Implications of neuronal diversity on population coding. Neural Comput 2006;18:1951–1986. [PubMed: 16771659]

Stevens CF. Neuronal diversity: too many cell types for comfort? Curr Biol 1998;8:R708–R710. [PubMed: 9778523]

Swain GP, Ayers J, Selzer ME. Metamorphosis of spinal-projecting neurons in the brain of the sea lamprey during transformation of the larva to adult: normal anatomy and response to axotomy. J Comp Neurol 1995;362:453–467. [PubMed: 8636461]

Szobota S, Gorostiza P, Del Bene F, et al. Remote control of neuronal activity with a light-gated glutamate receptor. Neuron 2007;54:535–545. [PubMed: 17521567]

Tanaka, T.; Joke, T.; Oka, T. Cell nucleus segmentation of skin tumor using image processing. Engineering in Medicine and Biology Society; Proceedings of the 23rd Annual International Conference of the IEEE; 2001. p. 2716-2719.

Tseng GF, Prince DA. Heterogeneity of rat corticospinal neurons. J Comp Neurol 1993;335:92–108. [PubMed: 8408775]

Urban J, Technau GM. Cell lineage and cell fate specification in the embryonic CNS of Drosophila. Semin Cell Dev Biol 1997;8:391–400. [PubMed: 15001077]

Van Den Elsen PA, Pol EJD, Viergever MA. Medical image matching-a review with classification. Eng Med Biol Mag, IEEE 1993;12:26–39.

Vincent L, Soille P. Watersheds in digital spaces: an efficient algorithm based on immersion simulations. IEEE Trans Pattern Anal Mach Intell 1991;13:583–598.

Westerfield, M. Danio rerio. Vol. 3. University of Oregon Press; Eugene, OR: 1995. The zebrafish book: a guide for the laboratory use of zebrafish.

Yen CT, Jones EG. Intracellular staining of physiologically identified neurons and axons in the somatosensory thalamus of the cat. Brain Res 1983;280:148–154. [PubMed: 6197137]

Zhang F, Wang LP, Boyden ES, Deisseroth K. Channelrhodopsin-2 and optical control of excitable cells. Nat Methods 2006;3:785–792. [PubMed: 16990810]

Zottoli SJ. Correlation of the startle reflex and Mauthner cell auditory responses in unrestrained goldfish. J Exp Biol 1977;66:243–254. [PubMed: 858992]

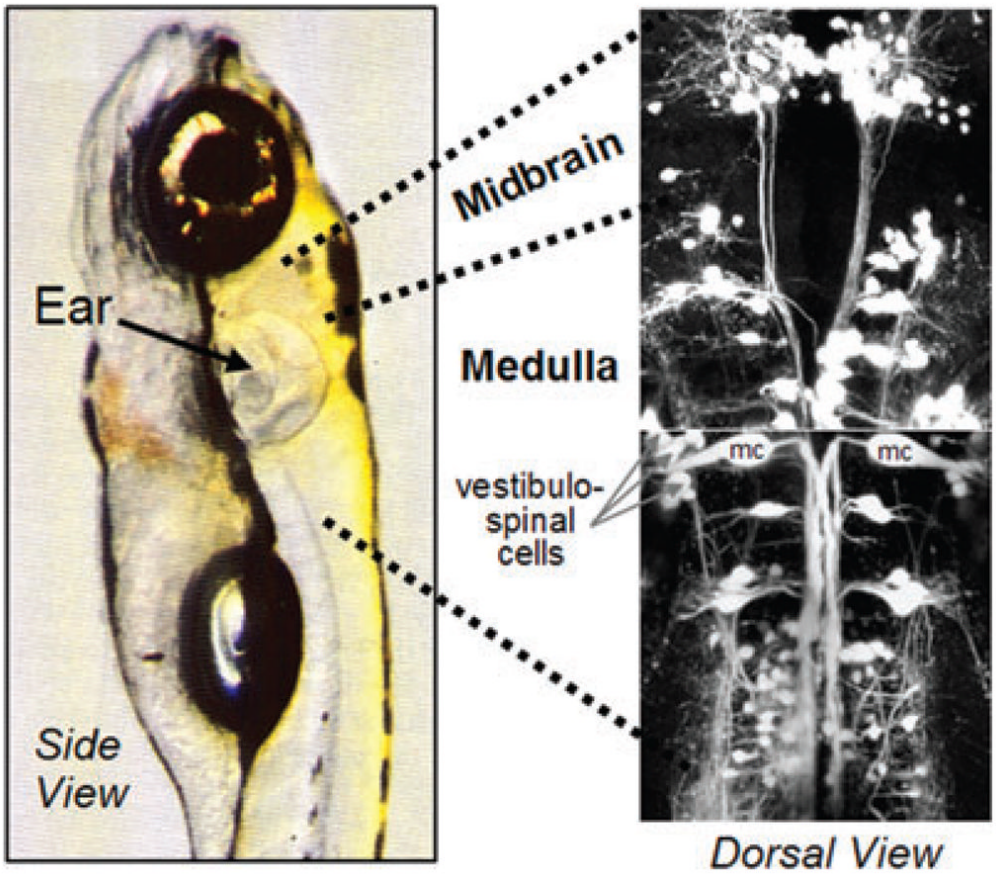

Fig. 1.

Orientation of confocal datasets. All datasets were acquired from the brainstem of restrained larval zebrafish (the brainstem is comprised of the medulla and midbrain in fishes). The lateral view of the larva illustrates very well the brain's transparency, but our 3D datasets are always collected from a dorsal view which provides a better layout of the reticulospinal neurons being studied. In addition, the larval ear obstructs much of the rostral medulla in the lateral view. Our dorsal-view confocal images are shown oriented with the head up and tail down. For orientation, the larval ears are just outside the vestibulospinal cells, which are found at the end of the lateral dendrites of the Mauthner cells on either side of the larval head.

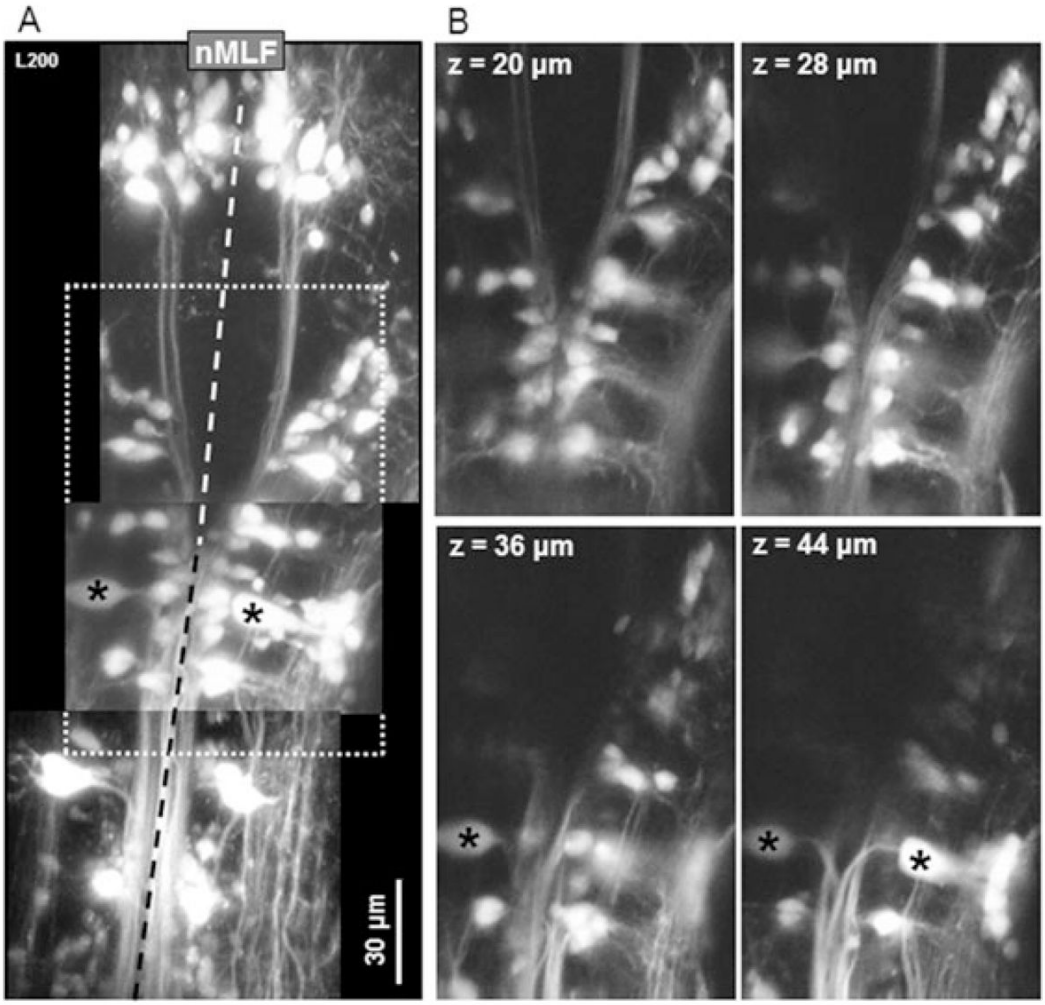

Fig. 2.

Example confocal dataset from a restrained larval zebrafish. A large population of neurons has been fluorescently labelled by retrograde transport of Oregon Green Dextran from spinal cord. Because neurons overlap one another in the *z*-dimension, 3D analysis is required to distinguish them. (A) Two large midbrain clusters (nMLF or nucleus of the longitudinal medial fasciculus) are present in rostral brainstem on either side of the larval midline (dashed line). The caudal brainstem shows a segmentally organized array of neurons spanning the medulla. This montage is constructed from maximum projection images of three confocal datasets, each with 16 optical sections acquired at 4-µm intervals. (B) Shown are four individual optical sections taken at different depths from the middle stack of the three stacks making up the montage. Note that these images extend beyond the portion shown in (A) because *z*-stacks are acquired with sufficient overlap for easy alignment into a continuous montage. The *xy*-extent of the middle image stack is indicated in by the dotted lines in (A). Asterisks mark the left and right Mauthner cells both in the montage (A) and in those image planes in (B) where the Mauthner cell bodies are evident. Scale bar = 30 µm.

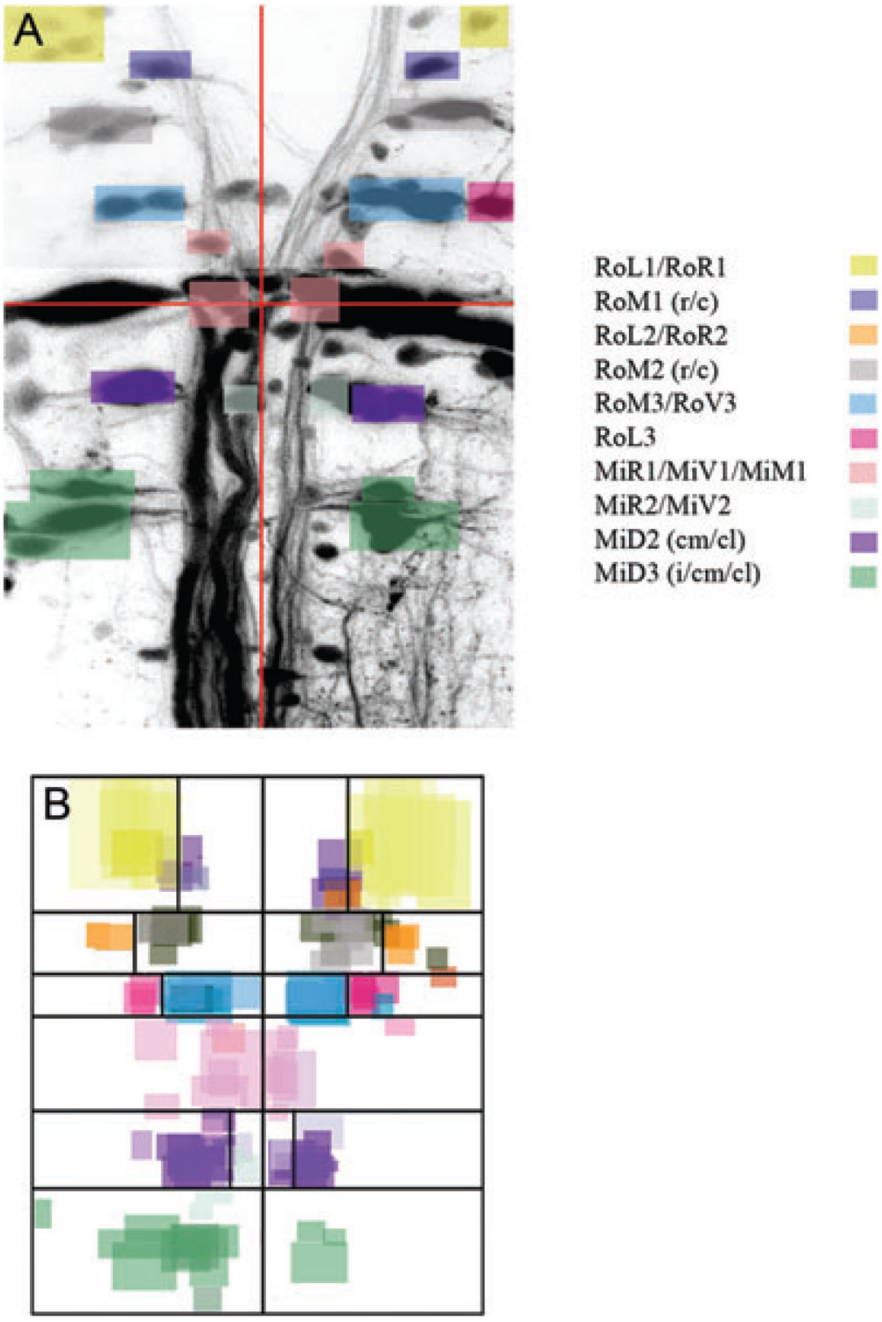

Fig. 3.

Construction of the DMCS template. (A) Starting from a montage of maximum projection images of confocal image stacks that spanned this larva's brainstem, we manually assigned identities to labelled descending neurons in accordance with prior descriptions (see tabulation in O'Malley *et al.*, 2003); these identifications are represented as colour-coded rectangles. This procedure was repeated for 11 zebrafish, each of which was represented by multiple confocal image stacks. (B) Because no confocal dataset has all 300 descending neurons labelled, we used a cumulative procedure to define the locations of all descending neurons into a common coordinate system. After colour coding all neurons, we used the 'layers' feature in Adobe Photoshop to project all represented neurons from all datasets into a single plane. Image

transformations (including rotation, translation, scaling and affine transformations) were used to conform all image sets into this common coordinate system (Broit, 1981; Brown, 1992). The colour intensity at each location represents the probability within this dataset of finding those specific neurons at that location in the template.

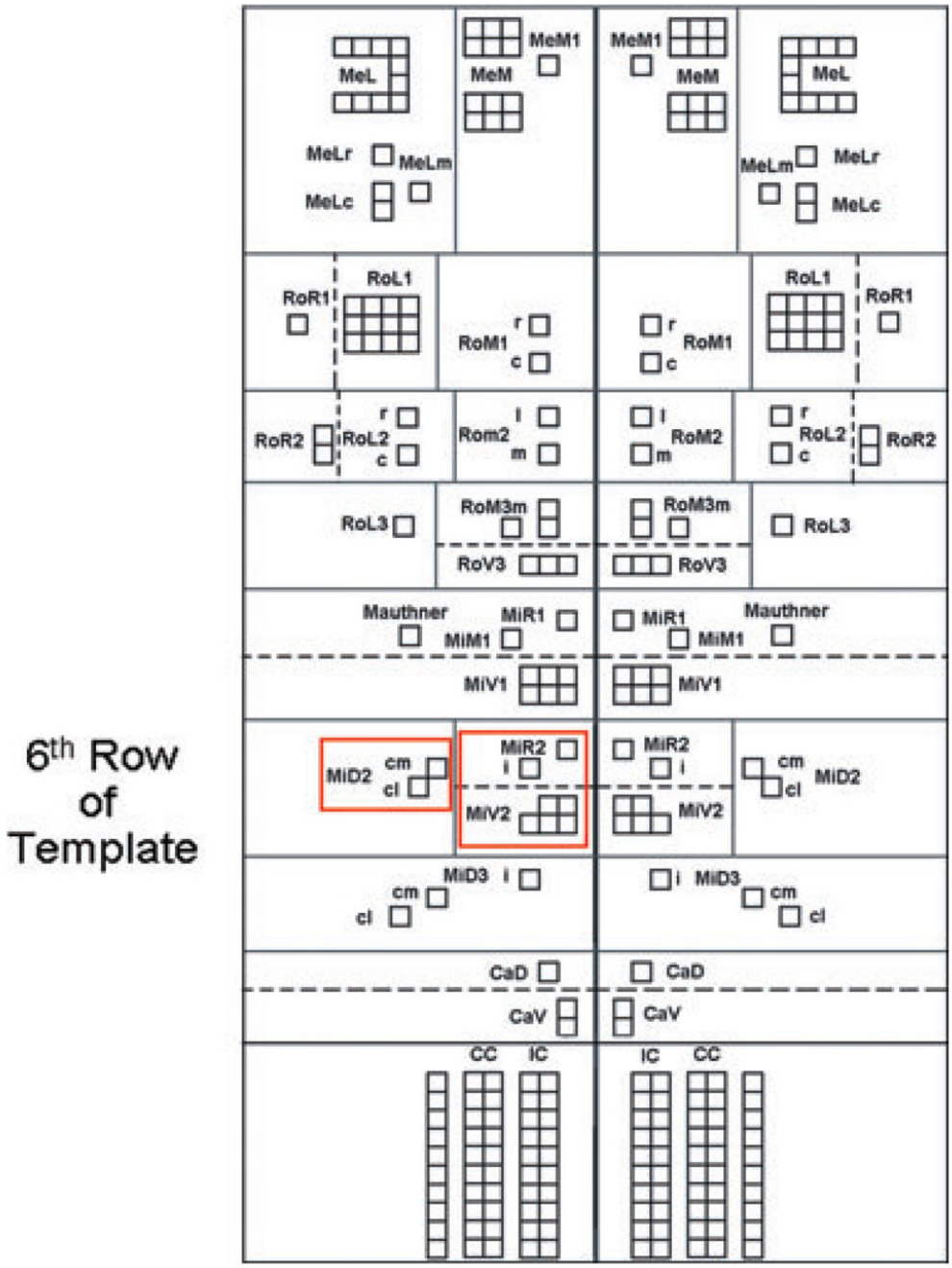

Fig. 4.

The DMCS template. Based on the method illustrated in Fig. 3, a template was constructed that includes the locations of all known reticulospinal neurons in the larval zebrafish brainstem. This template is organized into a set of zones and sub-zones and is used for automated cell identification. There are a total of 28 zones, 14 on each side. Some zones have only one neuronal cluster whereas others have two or three clusters. Six of the 14 unique zones were divided into two sub-zones to allow for more refined cell identification. This results in a total of 20 distinct regions in the template on each side of brainstem. Zones are bounded by solid lines, whereas sub-zones are separated by dashed lines. The red boxes on the sixth row of zones highlight an undivided zone (lateral box) and a sub-divided zone (medial box). In subsequent image

processing steps, automatically segmented neurons are assigned to zones based upon their location within the 3D confocal datasets. Note that a group of approximately 30–40 vestibulospinal neurons (not included in the template) makes up essentially the remainder of the 300 known descending neurons; these neurons have not been functionally subdivided and are easily recognized as a neuronal grouping distinct from the reticulospinal cells (see O'Malley *et al*., 2003).

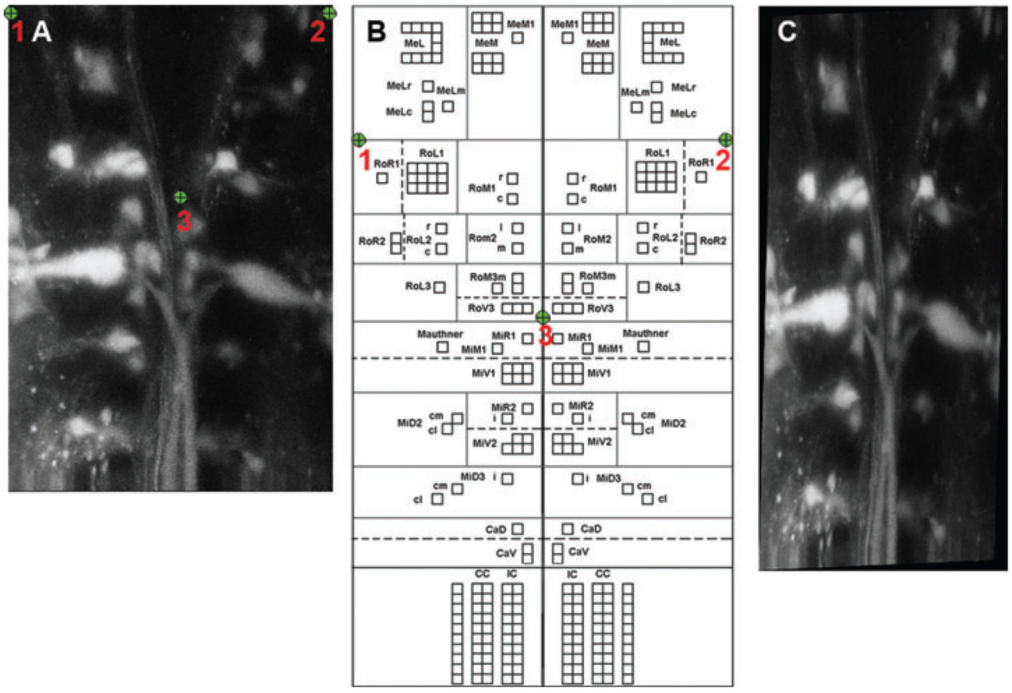

Fig. 5.

Registration of MIP images to the template coordinate system. To convert the confocal datasets to the template coordinate system, the user manually selects three registration points (green symbols) on the maximum intensity projection (A) of the dataset and clicks on three corresponding points in the DMCS template (B). Using an affine transformation, the entire 3D set of images is then warped into the normalized template space, as shown in a MIP projection in (C). This procedure proves suitably robust for this application in part because these confocal datasets have roughly similar orientations, based on the experimental positioning of the fish prior to data acquisition.

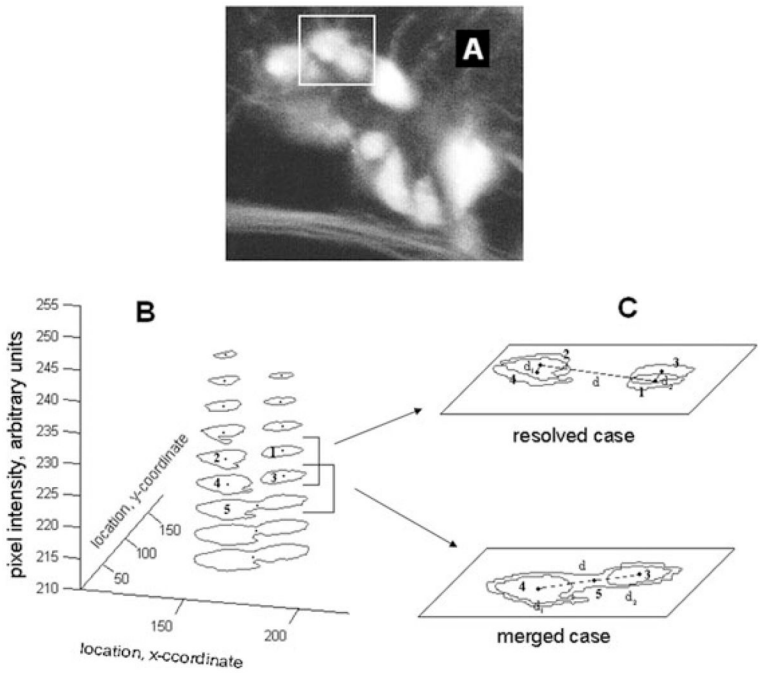

Fig. 6.

Segmentation of neuronal contours. Prior to identification, neurons must first be detected or 'segmented' as discrete objects. (A) Shows a confocal optical section in which there are densely packed neurons, including two (inside the white box) that appear to be touching one another. (B) and (C) illustrate segmentation of this pair of neurons. (B) As the pixel-intensity threshold is increased, a single merged object becomes two separate objects (marked with small dots). (C) Adjacent threshold-planes from (B) are projected to illustrate an abrupt change in centre-point location when two objects become merged. In the resolved case, the change in location of an object's centre is slight as one moves down one step in threshold. But at a certain step down (merged case), the two objects merge and there is an abrupt shift in centre location – the centres of the two objects (3 and 4) now move to become one common centre point of the merged contour (object 5). At this point, the contours in the immediately higher threshold plane (i.e. the 'pre-merged' contours) are taken as boundary contours of the two cells from this optical section.

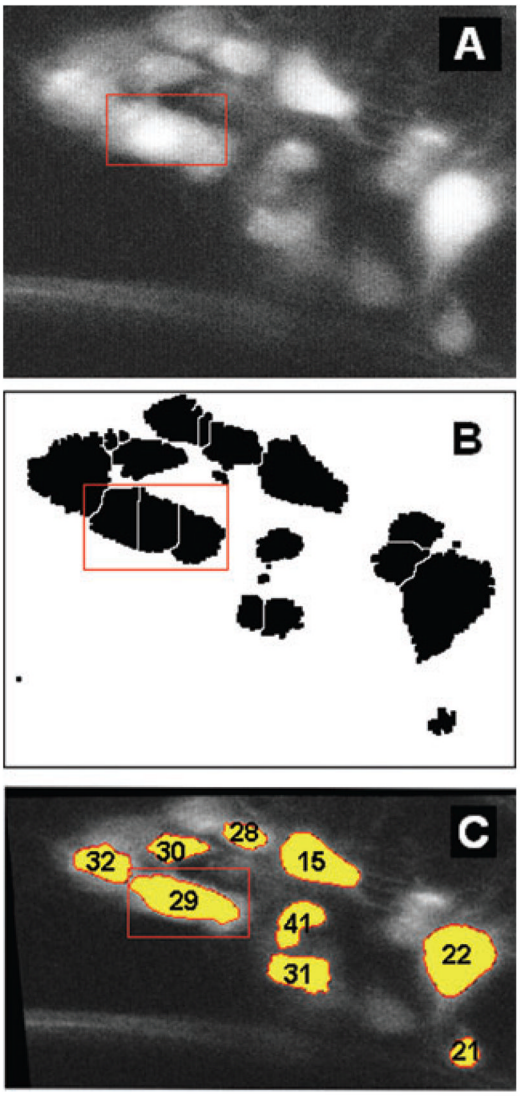

Fig. 7.

Alternative segmentation algorithms. (A) This representative optical section has many closely packed neurons that make their resolution difficult for both manual and automated identification procedures. (B) Using a conventional watershed algorithm, we see a large number of 'objects', e.g. the three distinct structures inside the red box. (C) Use of the boundary contour segmentation algorithm results in a segmentation of neurons that agrees better with the manual identification procedure. The numbering indicates individual neurons within the dataset to which the boundary contours shown have been assigned.

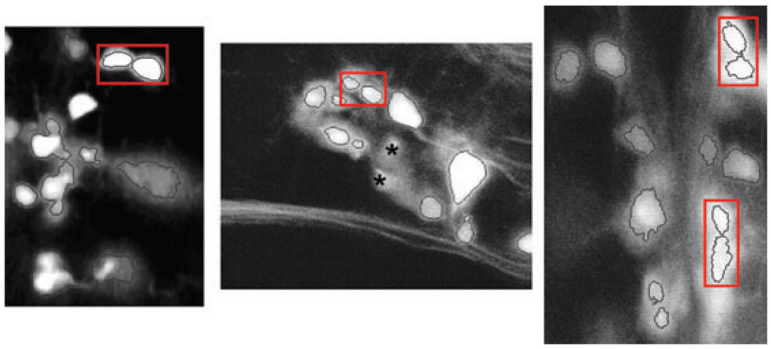

Fig. 8.

Example results of the boundary contour method. The grey contours are the boundary contours generated by the cell segmentation algorithm. In many instances neurons appear to touch – e.g. within the areas marked by red rectangles. In each of these instances, the neurons have been resolved in agreement with manual identification results. Note that some fluorescent structures, for example those indicated by asterisks (*) in the middle image, were not identified in this optical section as neurons, due to their failure to satisfy one or more inclusion criteria. At nearby sections in the image stack, these particular structures are seen to be continuous with segmented neurons.

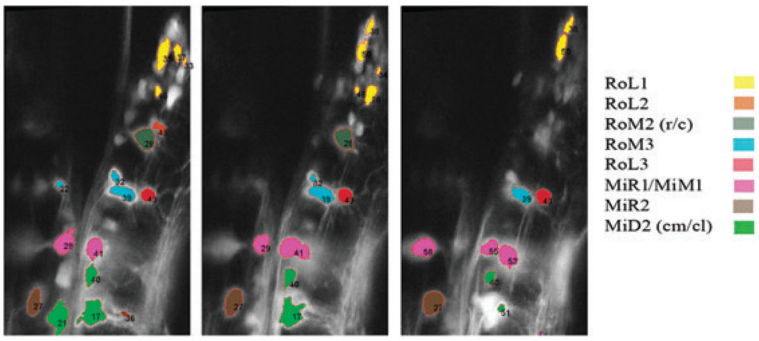

Fig. 9.

Output of the cell identification program. A graphical representation facilitates cross-checking of algorithm performance against manual identification. An example output is illustrated for three slices (slices #7, #8 and #9) from a 16-slice, annotated image stack. The segmented neurons are colour coded according to their zone assignment and each segmented neuron is given a unique identifying number. Overlaying the segmentation results onto the confocal *z*-stack allows the user to readily view the confocal, segmentation and identification results by simply using a slider button to navigate up and down through the dataset. This is useful in cases where the user wants to double-check cell assignments or make finer assignments within the template zones.

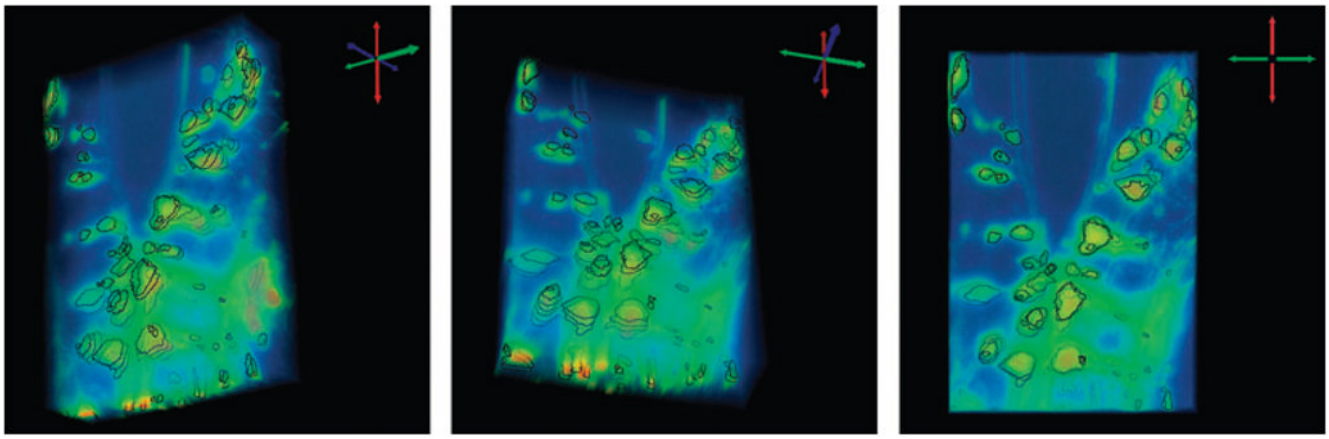

Fig. 10.

Visualization of datasets. 3D reconstructions of a sample dataset illustrate the distribution of boundary contours. Three distinct views of this same dataset are shown, with the blue arrow indicating the *z*-axis (which is approximately the dorsal-ventral axis) in each case. Note that the *z*-axis is stretched to make it easier to see the associated sets of boundary contours. The red arrow indicates the long axis of the larvae, whereas the green arrow runs along the medial-lateral dimension. The view on the right shows a dorsal view (i.e. the *xy* plane) and since the *z*-axis is perpendicular to this view of the reconstruction, the blue arrow that would indicate the *z*-axis is not visible. For each image, the sets of boundary contours generated in MatLab were imported using the SciRun/BioPSE software package (http://www.sci.utah.edu/cibc/software) and were meshed with the confocal data and projected as semi-transparent, 3D-renderings using the BioImage module. The linking of boundary contours across optical sections is central to the 3D segmentation and identification of neurons.

Table 1

Performance of the neuronal detection algorithm. The number of 'correctly segmented' neurons enumerates those neurons identified by both the manual and automated algorithms. Neurons detected manually, but not by the algorithm are designated as false negatives, whereas objects detected by the algorithm, but not manually are called false positives.

Fish #	# manually identified neurons	# of segmented neurons	# correctly segmented neurons	# of false positives	# of false negatives	# of unresolved neurons	# of mis-assigned neurons
191	43	41	38	3	5	0	2
193	38	37	31	6	7	0	0
199	87	92	82	10	5	2	1
200	68	68	59	9	9	1	0
203	19	13	10	3	9	1	0
204	69	51	46	5	23	1	2
205	37	39	33	6	4	0	2
207	57	53	50	3	7	0	0
211	36	44	36	8	0	0	3
212	39	42	33	9	6	1	0
214	44	41	36	5	8	0	2
Total	**537**	**521**	**454**	**67**	**83**	**6**	**12**

Table 2

Accuracy of neuronal assignment in the leave-one-out paradigm. Beginning with the number of correctly segmented neurons, the unresolved neurons are subtracted and then the number correctly assigned (i.e. in agreement with manual assignment) is determined. Subtraction of the correctly assigned neurons from the resolved neurons gives the number mis-assigned. The segmentation results are the same as for Table 1 because the segmentation algorithm is independent of the template/zone assignment algorithm.

Fish #	# of mis-assigned neurons
191	2
193	0
199	1
200	1
203	0
204	2
205	2
207	0
211	3
212	0
214	2
Total	**13**

Table 3

Example morphometric datasheet. Details on a cluster of MeL cells in the right midbrain are provided, including information on cell location (*x*, *y*, *z*) and size; locations are given in template coordinates.

MeL-R cell	*x*-coord.	*y*-coord.	*z*-coord.	Cell ID #	Width (pixels)	Length (pixels)
1	175.8	496.8	3.00	6	14.6	22.1
2	143.4	614.9	5.57	17	44.7	60.4
3	127.5	554.6	3.90	18	19.4	18.1
4	157.6	524.5	4.20	23	40.1	33.9
5	140.3	484.1	5.51	25	25.7	23.2
6	161.7	474.3	4.20	30	10.6	23.6
7	138.6	540.8	6.83	43	49.7	63.4
8	168.1	582.5	10.47	91	16.6	31.5